**Atmospheric
Chemistry
and Physics
Discussions**

Climate versus emission drivers of methane lifetime from 1860–2100

J. G. John[1], A. M. Fiore[1,*], V. Naik[2], L. W. Horowitz[1], and J. P. Dunne[1]

[1]Geophysical Fluid Dynamics Laboratory/NOAA, Princeton, NJ, USA
[2]UCAR/Geophysical Fluid Dynamics Laboratory, Princeton, NJ, USA
[*]now at: Department of Earth and Environmental Sciences, and Lamont-Doherty Earth Observatory of Columbia University, Palisades, NY, USA

Correspondence to: J. G. John (jasmin.john@noaa.gov)

Title Page

Abstract	Introduction
Conclusions	References
Tables	Figures

Back | Close

Full Screen / Esc

Printer-friendly Version

Interactive Discussion

Abstract

With a more-than-doubling in the atmospheric abundance of the potent greenhouse gas methane (CH_4) since preindustrial times, and indications of renewed growth following a leveling off in recent years, questions arise as to future trends and resulting climate and public health impacts from continued growth without mitigation. Changes in atmospheric methane lifetime are determined by factors which regulate the abundance of OH, the primary methane removal mechanism, including changes in CH_4 itself. We investigate the role of emissions of short-lived species and climate in determining the evolution of tropospheric methane lifetime in a suite of historical (1860–2005) and Representative Concentration Pathway (RCP) simulations (2006–2100), conducted with the Geophysical Fluid Dynamics Laboratory (GFDL) fully coupled chemistry-climate model (CM3). From preindustrial to present, CM3 simulates an overall 5 % increase in CH_4 lifetime due to a doubling of the methane burden which offsets coincident increases in nitrogen oxide (NO_x) emissions. Over the last two decades, however, the methane lifetime declines steadily, coinciding with the most rapid climate warming and observed slow-down in CH_4 growth rates, reflecting a possible negative feedback through the CH_4 sink. The aerosol indirect effect plays a significant role in the CM3 climate and thus in the future evolution of the methane lifetime, due to the rapid projected decline of aerosols under all four RCPs. In all scenarios, the methane lifetime decreases (by 5–13 %) except for the most extreme warming case (RCP8.5), where it increases by 4 % due to the near-doubling of the CH_4 abundance, reflecting a positive feedback on the climate system. In the RCP4.5 scenario changes in short-lived climate forcing agents reinforce climate warming and enhance OH, leading to a more-than-doubling of the decrease in methane lifetime from 2006 to 2100 relative to a simulation in which only well-mixed greenhouse gases are allowed to change along the RCP4.5 scenario (13 % vs. 5 %) Future work should include process-based studies to better understand and elucidate the individual mechanisms controlling methane lifetime.

1 Introduction

Atmospheric methane (CH_4) is the second most important anthropogenic greenhouse gas after carbon dioxide (CO_2), reflecting its stronger heat-trapping efficiency (100-yr global warming potential of 25) and more-than-doubling in abundance since pre-industrial times (Forster et al., 2007). As a precursor to global tropospheric ozone (O_3) (e.g. Prather et al., 2003), the third most important greenhouse gas, methane exerts an additional indirect influence on climate (Shindell et al., 2005), as well as on background levels of surface O_3 (Fiore et al., 2002), with corresponding adverse impacts on human health (West et al., 2006). We examine here the role of changes in emissions versus climate on atmospheric methane lifetime evolution on decadal-to-century time scales.

The contemporary methane budget includes both natural and anthropogenic sources. The largest natural source of methane is wetlands, with smaller contributions from termites, oceans and methane hydrates. Anthropogenic CH_4 sources include rice paddies, ruminants, coal and natural gas, landfills and biomass burning – together these account for over 60 % of the present-day global budget (Table 7.6 in Denman et al., 2007). The major sink of methane is oxidation by the hydroxyl radical (OH) in the troposphere (Levy, 1971), with smaller losses from absorption by soils, stratospheric destruction, and possible oxidation by atomic chlorine in the marine atmospheric boundary layer (Allan et al., 2005). While the global sources and sinks of methane are fairly well known and currently in approximate balance (annual source and sink strengths estimated at 582 Tg CH_4 and 581 Tg CH_4, respectively, Denman et al., 2007), uncertainties exist in their trends and in the contributions from individual source sectors.

Prior studies have established the dominant role of the tropical lower troposphere in oxidation of CH_4 due to high OH abundance and temperatures (as the CH_4 + OH reaction rate constant is strongly sensitive to temperature, $\sim 2\,\%\,K^{-1}$) (Logan et al., 1981; Prather and Spivakovsky, 1990; Crutzen and Zimmermann, 1991; Crutzen et al., 1999; Spivakovsky et al., 2000), with estimates ranging from 75 %–78 % CH_4 loss in the

tropics and 79 %–90 % CH$_4$ loss below 500 hPa (Spivakovsky et al., 2000; Lawrence et al., 2001; Fiore et al., 2008). Using OH estimates constrained by methyl chloroform (CH$_3$CCl$_3$) measurements for the period 1978–2005, Prinn et al. (2005) derived a methane lifetime of $10.2^{+0.9}_{-0.7}$ yr due to tropospheric OH loss. Dentener et al. (2003) used a chemistry-transport model to calculate a global average tropospheric lifetime of 9.0 ± 0.13 yr for the period 1979–1993, while Stevenson et al. (2006) obtained a present-day total lifetime of 8.67 ± 1.32 yr from a multi-model ensemble study; the multi-model range in total lifetimes in the latter study implies a lifetime range of $9.90^{+1.68}_{-1.76}$ yr with respect to tropospheric OH.

The OH abundance and distribution reflect a complex interplay among various factors including anthropogenic and natural emissions, as well as meteorological processes that may change with climate. Increases in atmospheric CH$_4$ burden, carbon monoxide (CO), and non-methane volatile organic compounds (NMVOCs) all act to decrease OH concentrations and increase the methane lifetime. Increases in UV (photolysis frequencies viz. J(O^{1}D)), water vapor (H$_2$O), and nitrogen oxide (NO$_x$) sources tend to increase OH, which in turn decreases the atmospheric lifetime of methane. The non-linearities in OH chemistry complicate definitive attributions to individual processes controlling OH (e.g. Spivakovsky et al., 2000).

Since the pre-industrial period, the concentration of methane in the atmosphere has risen rapidly from about 700 ppb (Flückiger et al., 2002) in 1750, to a present-day value of nearly 1800 ppb. There is as yet no consensus, however, on the change in methane lifetime during this period, with estimates ranging from a 14 % decrease to a 34 % increase (cf. Table 1). This wide range reflects uncertainty in the sign of changes in OH concentrations since the pre-industrial. For example, Staffelbach et al. (1991) inferred a 30 % decrease in polar regions based on ice-core measurements of formaldehyde (CH$_2$O), while model estimates suggest smaller decreases or even increases globally (Table 1).

While observations could theoretically provide constraints on OH trends over recent decades (Dlugokencky et al., 1998; Spivakovsky et al., 2000; Prinn et al., 2005),

Title Page

Abstract | Introduction

Conclusions | References

Tables | Figures

◄ | ►

◄ | ►

Back | Close

Full Screen / Esc

Printer-friendly Version

Interactive Discussion

attributing small changes (a few percent of the large CH_4 atmospheric abundance) unambiguously to the many individual processes exerting multiple competing influences on OH is complicated. For example, Krol et al. (1998) report a positive OH trend of 0.46 % yr^{-1} from 1978–1993 due to combination of stratospheric O_3 loss, reduced carbon monoxide concentrations, and increases in water vapor abundance and NO_x emissions, while Dentener et al. (2003) attribute an increase in OH trend from 1979–1993 to water vapor in the tropical troposphere (Table 2).

The growth rate of atmospheric methane increased steadily until 1990, after which it declined (Dlugokencky et al., 1998), leading to a leveling off from 1999 to 2007. Observations suggest that the atmospheric methane concentration since 2007 is once again on the rise (Rigby et al., 2008). Attribution of the slow-down in growth rate during the 1990s is quite complicated as the changes are small and there are many competing influences at work. Hypotheses to explain the observed CH_4 trends in recent decades have ranged from a steady-state equilibrium of methane sources and sinks (Dlugokencky et al., 1998), to decreases in natural and/or anthropogenic emissions (e.g. Kai et al., 2011), as well as variations in meteorological factors and processes (e.g. Fiore et al., 2006; Hodson et al., 2011; cf. Table 2).

Here we investigate the relative importance of changes in anthropogenic emissions versus climate in contributing to changes in the methane lifetime from 1860 to 2100 in the context of the new set of historical and future emission scenarios (Lamarque et al., 2010; Meinshausen et al., 2011; van Vuuren et al., 2011a) developed for the fifth phase of the Coupled Model Intercomparison Project (CMIP5) (Taylor et al., 2012), in support of the Intergovernmental Panel on Climate Change (IPCC) Fifth Assessment (AR5). We use a state-of-the-art global fully coupled climate-chemistry model, the Geophysical Fluid Dynamics Laboratory Coupled Model version 3 (CM3) to examine the drivers and trends of tropospheric methane lifetime under these scenarios. This new tool allows for a broader suite of chemistry-climate interactions and our analysis is a prelude to further multi-model comparisons such as those occurring under the Atmospheric Chemistry and Climate Model Intercomparison Project (ACCMIP) in support of IPCC AR5.

2 Model description and simulations

The Geophysical Fluid Dynamics Laboratory CM3 Model incorporates an atmospheric chemistry model within the fully interactive framework of the atmosphere, ocean, land, and sea-ice components (Donner et al., 2011; Naik et al., 2012; Griffies et al., 2011; C. Milly, personal communication, 2012; Shevliakova et al., 2009). We provide here a summary of the features most relevant to the simulation of OH.

The CM3 model simulates interactive tropospheric and stratospheric chemistry, achieved by merging the mechanisms from MOZART-2 (Horowitz et al., 2003) and AM-TRAC (Austin and Wilson, 2006), respectively, as described by Naik et al. (2012) who evaluate global trace gas distributions over recent decades with in situ measurements of O_3 and other OH precursors. The model simulates atmospheric concentrations of 97 chemical species, 12 of which are aerosol species. Photolysis rates are not directly affected by changes in aerosols, except through clouds. Global mean CH_4 and nitrous oxide (N_2O) concentrations are restored with a timestep of 1 day, to a lower boundary condition (below 800 hPa) for chemistry. The impact of climate change on CH_4 emissions from wetlands (and any other natural sources); from wildfires; and from other biogenic precursors to OH which can influence the CH4 lifetime (such as NMVOC and soil nitrogen oxide emissions), are not included. Inclusion of these feedbacks would likely alter the findings here, though uncertainties are large (Arneth et al., 2010). The model applies climatological biogenic isoprene and soil NO_x emissions as in Horowitz (2006). Lightning NO_x (LNO_x) is the only natural source that is tied to the model meteorology and thus can respond to changes in climate. The parameterization of both continental and oceanic lightning NO_x is based on empirical relationships between convective cloud top heights and lightning flash frequencies as in Horowitz et al. (2003), Price et al. (1997) and Levy et al. (1996).

Table 3 provides a summary of the CM3 model simulations analyzed here. A multi-century 1860 Control integration (CONTROL) using prescribed (static) vegetation and constant 1860 land use fractions was performed initially, and five historical ensembles

Climate versus emission drivers of methane lifetime

J. G. John et al.

Full Screen / Esc

Printer-friendly Version

Interactive Discussion

(HIST) were branched from CONTROL after achieving a stable, realistic climate (L. Horowitz, personal communication, 2012). Both vegetation dynamics and land use (defined as land use change plus harvesting) were activated in the land model component of CM3 for all historical simulations and future projections.

In addition to the historical model ensemble where all forcings vary in time as described by Lamarque et al. (2010), additional "single-forcing" experiments were conducted in which an individual forcing is allowed to vary with time, with other forcings held constant at 1860 levels. The specifications for these 3-member ensemble simulations, viz. AEROSOL, AEROSOL INDIRECT, ANTHRO, NATURAL, and WMGGO3, are described in Table 3. In AEROSOL INDIRECT, aerosol and aerosol precursor emissions vary as in HIST, but an 1860 climatology taken from years 1–20 of CONTROL is used for radiation. The difference between the AEROSOL and AEROSOL INDIRECT simulations therefore reflects the contribution from the aerosol direct effect. Land use fractions are held at 1860 values (i.e. there are no land use transitions) in AEROSOL, AEROSOL INDIRECT, NATURAL and WMGGO3. CO_2 concentrations for radiation and land plant photosynthesis are held constant at the 1860 value of 286.15 ppm in AEROSOL, AEROSOL INDIRECT and NATURAL. These simulations can be used to investigate key drivers of overall historical changes, to isolate the "forced" response (i.e., to anthropogenic emissions), and to separate climate drivers (temperature, H_2O, $J(O^1D)$, lightning NO_x) from anthropogenic emission drivers (CO and NO_x emissions, CH_4 concentrations) of methane lifetime within time periods.

Future projections use time-varying forcings as recommended for the new Representative Concentration Pathways (RCPs) scenarios developed for CMIP5 in support of IPCC AR5 (Table 3). The year 2100 radiative forcing (RF) of the four projection pathways ranges from 2.6 to 8.5 W m^{-2} (Moss et al., 2010). At the low end, RCP2.6 (also called RCP3-PD) is a peak and decline scenario, with greenhouse gas emissions peaking early in the century and then declining thereafter (van Vuuren et al., 2011b). In this scenario, RF peaks at ~3 W m^{-2} mid-century and then falls to 2.6 W m^{-2} by 2100. The two intermediate scenarios, RCP4.5 (Thomson et al., 2011) and RCP6.0 (Masui et al.,

Climate versus emission drivers of methane lifetime

J. G. John et al.

2011) are stabilization without overshoot pathways, with total RF reaching $4.5\,\mathrm{W\,m^{-2}}$ and $6.0\,\mathrm{W\,m^{-2}}$ respectively at stabilization (2100). The most drastic warming scenario is RCP8.5 which has rapidly increasing greenhouse gas emissions throughout the next century, and reaches a RF of $8.5\,\mathrm{W\,m^{-2}}$ by 2100 (Riahi et al., 2011).

5 CH_4 emissions (and concentrations) peak in 2010 and then decline rapidly in RCP2.6; are relatively stable, but higher, in RCP4.5 and RCP6.0; and rise rapidly to significantly higher values in RCP8.5. In all four RCP scenarios, emissions of aerosols and their precursors, as well as of non-methane OH precursors (i.e., NO_x, NMVOC, CO) are assumed to decline, under the assumption of aggressive air pollution abate-
10 ment strategies (van Vuuren et al., 2011a). An additional 3-member model ensemble (RCP4.5*), identical to RCP4.5, but with aerosol emissions, O_3 precursors, CH_4, N_2O and ozone-depleting substances (ODS) for chemistry held at year 2005 values, enables us to isolate the role of a warming climate from that of emission changes of chemically active species on the methane lifetime evolution under the RCP4.5 scenario. Compar-
15 isons across these scenarios can yield process-level insight into the factors dominating the methane lifetime evolution over the next century.

3 Approach

We define the global annual mean lifetime of methane against tropospheric OH, τ_{CH_4}, as the quotient of the global total atmospheric methane burden $[CH_4]$, and the globally
20 integrated tropospheric CH_4 loss rate, $k(T)\,[OH][CH_4]$:

$$\tau_{CH_4} = \frac{\int_{surface}^{TOA}[CH_4]}{\int_{surface}^{tropopause} k(T)\,[OH][CH_4]} \tag{1}$$

where the rate constant, $k(T) = 2.45 \times 10^{-12} e^{-1775/T}$ $(\mathrm{molec^{-1}\,cm^{-3}\,s^{-1}})$ is from JPL 2006 (Sander et al., 2006). The tropopause level is defined as the 150 ppbv O_3 level in

year 1860 of the appropriate historical ensemble member, and is applied to all simulation years.

Results are averaged over ensemble members where available. For our 1860 CONTROL simulation (Table 3), the mean and standard deviation of τ_{CH_4} averaged over 200 yr is 8.06 ± 0.08 yr, which is within the range of preindustrial estimates (6.71–12.8 yr) simulated by other models (Martinerie et al., 1995; Unger et al., 2009; Sövde et al., 2011). Figure 1 shows the temporal evolution of the global annual mean tropospheric methane lifetime in the CM3/CMIP5 historical simulations and future projections, and in Table 4 we report the mean and standard deviation of τ_{CH_4}, as well as the correlation coefficient of τ_{CH_4} with the global mean lower tropospheric (below 500 hPa) airmass-weighted OH concentration and temperature, over the full length of the model simulations.

Globally, percent changes in the reaction rate constant (Δk) and in OH abundances in the lower tropical troposphere (ΔOH) should sum to the magnitude of the overall percent change in methane lifetime ($\Delta\tau_{CH_4}$), as confirmed in Fig. 2 which shows the linearity between these terms, obtained by differencing 20-yr averages from the start and end of the various model simulations ($r^2 = 0.99$). In Table 5 we present the temperature change, along with percent changes of τ_{CH_4}, k, OH, CH_4, CO emissions, surface NO emissions, LNO_x and $J(O^1D)$ over 20-yr periods at the beginning and end of the model simulations, noting the non-linear interactions of the individual processes in contributing to the net changes in OH, while Table 6 reports the correlations of OH with CH_4, CO emissions, surface NO emissions, the lightning NO_x source (which is not included in the total surface NO emissions), lower tropospheric O_3 photolysis rates and stratospheric O_3 over the full model simulation periods (146 yr for historical and 95 yr for RCPs).

Below, we examine the overall drivers of simulated changes in methane lifetime. We further select a few time periods as illustrative examples to separate the roles of changes in climate and anthropogenic emissions in determining the lifetime of methane.

4 Historical period (1860–2005)

We first separate the anthropogenic forcing from natural variability by comparing the HIST and ANTHRO ensembles (Table 3). We then further separate ANTHRO into influences from aerosol versus well-mixed greenhouse gas by comparing AEROSOL (and
5 AEROSOL INDIRECT) with WMGGO3.

4.1 Overall drivers of methane lifetime

For the HIST five-member ensemble, the global mean tropospheric methane lifetime over the period 1860 to 2005 is 8.63 ± 0.24 yr (Table 4), with an overall 5 % increase from 1860–1879 to 1986–2005. τ_{CH_4} is strongly anti-correlated with the global mean
10 airmass-weighted OH below 500 hPa (Table 4), which shows an almost 6 % decrease from 1860–1879 to 1986–2005 (Table 5). In a sensitivity simulation in which only emissions of NO_x, CO, NMVOC, and aerosols (or their precursors) increase from 1860 to 2000, Naik et al. (2012) find a 14 % decrease in methane lifetime from preindustrial to present. We therefore attribute the increase in τ_{CH_4} solely to the doubling of the global
15 methane burden in HIST, which offsets the shortening of τ_{CH_4} due to the quadrupling of NO_x emissions (Table 5). The warming over the historical period has little impact, as demonstrated by the weak correlation with temperature in Table 4.

The "single-forcing" simulations (Table 3) provide additional insights into the relative importance of individual processes in driving the changes in HIST. The lifetime in-
20 creases in all of the single-forcing simulations, with the exception of WMGGO3 where τ_{CH_4} decreases by 4.3 % (Table 5, Fig. 1). The consistency of the overall τ_{CH_4} changes between ANTHRO and HIST confirms the dominant role of anthropogenic drivers, as opposed to natural forcings, in shaping the τ_{CH_4} evolution over the historical period. The percent change in the methane loss rate due to the temperature dependence of the re-
25 action rate constant from 1860–1879 to 1986–2005 in ANTHRO is almost double that of HIST (1.4 % vs. 0.8 % in Table 5), as there is no cooling effect from volcanoes. Despite this stronger temperature effect on ANTHRO, the percent increase in the lifetime of

CH_4 is comparable to that of HIST due to an offsetting larger decrease in OH (Table 5, Fig. 3b). Correlations of OH with CO emissions, CH_4 and $J(O^1D)$ (Table 6) are stronger in ANTHRO as the "forced" signal in HIST is masked by natural variability (e.g. volcanoes) to some extent. Without the effects of natural forcings, the average τ_{CH_4} over the period 1860 to 2005 is 2.2 % lower (compare ANTHRO with HIST in Table 4).

The largest increases in τ_{CH_4} from 1860–1879 to 1986–2005 occur in the AEROSOL and AEROSOL INDIRECT simulations (∼7 % each in Table 5). These larger increases as compared to HIST are driven entirely by aerosol-induced climate feedbacks on both temperature and OH, with the OH impact on τ_{CH_4} almost double that of the temperature effect (Table 5). The overall reduction in OH can be attributed solely to climate change in response to aerosol increases over the historical period because the CH_4 burden and emissions of CO and NO are held constant at 1860 values in these simulations (Table 3). OH concentrations in AEROSOL and AEROSOL INDIRECT strongly correlate with lightning NO_x, water vapor and $J(O^1D)$ (all below 500 hPa) (Table 6). The consistency between the AEROSOL INDIRECT and AEROSOL in the evolution of tropospheric methane lifetime (identical correlations of τ_{CH_4} against temperature and OH below 500 hPa in Table 4; similar percentage changes in Table 5 and correlations of OH versus the climate factors in Table 6), imply that aerosol-cloud interactions (indirect effect) dominate the CM3 climate response to aerosols (L. Horowitz, personal communication, 2012). τ_{CH_4} in our model is therefore sensitive to the aerosol indirect effect (Unger et al., 2009).

In ANTHRO, aerosol-induced cooling is offset by increases in temperature and OH associated with rising greenhouse gases (Fig. 3). Indeed, τ_{CH_4} is considerably shortened in WMGGO3 due to a large warming (Fig. 3a), which leads the CH_4 + OH reaction rate constant to increase by factors of about 6 and 3.3, respectively, compared to HIST and ANTHRO (4.6 % vs. 0.8 % and 1.4 % in Table 5). In this ensemble, the changes in CH_4 burden, CO and NO emissions are the same as in HIST and ANTHRO (Tables 3, 5), but rising temperatures (∼2K by 2005) – and the associated rise in water vapor, along with a 4.6 % increase in LNO_x in the model, both of which increase OH,

serve to drive τ_{CH_4} down (Table 5), so that the lifetime of methane is markedly reduced in WMGGO3. The single-forcing experiments thus serve to illustrate that the overall changes in HIST and ANTHRO reflect a complex balance among several opposing influences on temperature and OH, both of which determine the overall τ_{CH_4} evolution.

4.2 Selected periods within the historical simulations

Although we conclude that CH_4 anthropogenic emissions drive the overall changes in τ_{CH_4} from 1860 to the present, climate feedbacks are evident for specific time periods in HIST. Following volcanic events such as Krakatoa (1883), Agung (1963), El Chichón (1982) and Pinatubo (1991), methane lifetime peaks (Fig. 1), resulting from strong stratospheric aerosol-induced cooling in the model and the associated decrease in water vapor (Figs. 3a, 4b). OH is reduced as a result of the lower atmospheric humidity, as well as decreases in lightning NO_x (Fig. 4a); with minima in temperature, OH, water vapor and LNO_x coinciding with the peak methane lifetimes occurring in 1884, 1965, 1983 and 1992.

In WMGGO3, the wide scatter of τ_{CH_4} with OH over the full simulation period (slope = −0.1) arising from changes in the slope of τ_{CH_4} (due to different rates of change of temperature and OH) from 1860–1920, 1921–1970, and 1971–2005, results in an absence of overall correlation (Table 4). Temperature and associated water vapor rise gradually initially, and then more sharply after the 1960s. From 1921–1970, increasing CO emissions, CH_4 burden and decreasing photolysis rates drive OH down, counterbalancing the competing influences of rising temperature, water vapor, NO and LNO_x. In the late 20th century, τ_{CH_4} falls continuously as temperature and water vapor continue to rise even more rapidly (Fig. 3a, 4b).

4.3 Trends in recent decades

Over the last 20 yr of HIST τ_{CH_4} declines steadily, coinciding with the period of most rapid warming, suggesting a negative climate feedback since rising temperature and

water vapor shorten τ_{CH_4} (Bekki and Law, 1997; Johnson et al., 2002; Dentener et al., 2003; Fiore et al., 2006). Since the 1970s, we also note an increase in $J(O^1D)$ – presumably driven by depletion of stratospheric ozone (Fig. 4c, d) as aerosol changes do not directly affect photolysis rates in these simulations – which also enhances OH formation and shortens τ_{CH_4}. From 1998–2005, τ_{CH_4} continued to fall as stratospheric O_3 and $J(O^1D)$ levelled off, indicating that these factors were not contributing to the OH changes during this period. By 2005, τ_{CH_4} in HIST falls to ANTHRO, perhaps in part due to the lack of major volcanic eruptions since Pinatubo.

From 1979–1993, we obtain a global annual mean CH_4 lifetime versus tropospheric OH of 8.96 ± 0.09 yr, in good agreement with the Dentener et al. (2003) value of 9.0 ± 0.13 yr. The corresponding global airmass-weighted OH concentration below 500 hPa is $(1.28 \pm 0.007) \times 10^6$ molec cm^{-3}. The slight positive trend of 0.07% yr^{-1} over the period is smaller than the value of $0.24 \pm 0.06\%$ yr^{-1} reported by Dentener et al. (2003). The positive OH trend in recent decades in CM3 is in agreement with results from the current generation of modeling studies (Table 2), but is inconsistent with the negative OH trend and low interannual variability inferred from observations of CH_3CCl_3 (e.g. Bousquet et al., 2005; Montzka et al., 2011).

Similar to HIST, τ_{CH_4} in ANTHRO continues to fall over the last 20 yr, likely due to increasing water vapor (Fig. 4b). After 1980, increasing temperatures, water vapor and OH concentrations shorten CH_4 lifetime in ANTHRO, while cooling and decreasing OH in AEROSOL have the opposite effect, causing the lifetime to increase. Stratospheric ozone rises slightly in AEROSOL after 1990, as opposed to the strong decrease in ANTHRO; by 2005 τ_{CH_4} in AEROSOL exceeds that in ANTHRO by 0.42 yr (Fig. 1). After 1985, increased $J(O^1D)$ in WMGGO3, correlated with the depletion of stratospheric ozone, along with rising temperatures and water vapor (Fig. 3a, 4b) cause τ_{CH_4} to decrease steadily as in HIST, for an overall 4% decline over the period 1971–2005. In all the single-forcing simulations except for AEROSOL and AEROSOL INDIRECT, the

Full Screen / Esc

Printer-friendly Version

Interactive Discussion

climate drivers (rapid warming and associated increase in water vapor) dominate in the late 20th century, and the methane lifetime decreases.

Our historical and single-forcing experiments over the 1860–2005 period illustrate the diverse factors influencing the evolution of the methane lifetime, with cooling from aerosol-cloud interactions masking the effects of greenhouse gas warming over the historical period in CM3. Rising temperatures and increases in water vapor and LNO_x drive τ_{CH_4} down (Tables 4, 5) in WMGGO3. In contrast, the temperature-driven changes in reaction rate constant, water vapor and lightning NO_x are of the opposite sign in AEROSOL (Table 5) and τ_{CH_4} increases. Both climate and emissions influence the simulated methane lifetime in HIST; while emission-driven changes dominate the overall increase in τ_{CH_4} from the pre-industrial to present, climate warming in the late 20th century shortens the lifetime of CH_4. The aerosol indirect effect plays a major role in CM3 and its impacts on changes in methane lifetime need further investigation. The discrepancy between model and observationally based studies of CH_4 and OH trends in recent decades continues to be an unresolved puzzle. Since OH is expected to increase in a warming climate, the disagreement may indicate a problem with inferred OH trends, or some offsetting influence in chemistry, climate or emissions not represented in the models.

5 Future scenarios (2006–2100)

We focus first on the three RCP scenarios (RCP2.6, RCP4.5 and RCP6.0) that have equivalent decreases in anthropogenic NO_x emissions (∼45 %) by the end of the century (Table 5). The trajectory of τ_{CH_4} in RCP2.6 (Fig. 1) initially drops, reaching a minimum value of 7.22 yr in 2063, after which it rebounds, for an overall 9.1 % decrease from 2006–2025 to 2081–2100. In this "low warming" scenario, the associated temperature change below 500 hPa over the same time periods is ∼1.1 K, while lower tropospheric OH increases by 7.3 % (Table 5, Fig. 3), with both factors contributing to the decrease in τ_{CH_4}. The increase in OH concentration reflects increases in water

vapor, lightning NO_x, and $J(O^1D)$, and is further enhanced by reductions in CH_4 burden and CO emissions (Table 5), which together outweigh the 46 % reduction in total NO emissions. Prior to 2063, OH rises rapidly, driven by almost linear declines in methane burden and CO emissions (Fig. 5a, b). After 2063, τ_{CH_4} increases as the evolution of OH reverses and starts decreasing, driven by declining anthropogenic NO emissions, which offset the combined impacts on OH from warming and declining anthropogenic CO emissions.

Under the moderate warming scenario, RCP4.5, there is a linear decline in the lifetime of methane, which drops by 13 % from 2006–2025 to 2081–2100, the largest overall decrease in methane lifetime in any of the RCP projections (Fig. 1). Although the decrease in methane burden is only one-third that in RCP2.6 (Table 5), the larger increases in water vapor and lightning NO_x (driven by warming which is twice as large in RCP4.5 as compared to RCP2.6) combined with a larger decrease in CO emissions lead to an overall larger OH change by the end of the century than in RCP2.6. The overall warming in RCP4.5 is closer to that in RCP6.0 but the OH change in RCP4.5 is closer to that in RCP2.6, illustrating the complex interplay of climate and emissions in determining methane lifetimes.

We next explore the role of short-lived aerosol and ozone precursors in contributing to the climate-driven changes by comparing RCP4.5 with RCP4.5* (where the short-lived species are held at 2005 levels (Fig. 5), as are CH_4, N_2O and ODS for chemistry, but well-mixed greenhouse gases follow the RCP4.5 scenario, Table 3). In RCP4.5*, we again find a shortening of τ_{CH_4}, but the percent change is not as large as in the RCP4.5 ensemble – here roughly equal percent changes in rate constant and OH contribute to a 5 % reduction in methane lifetime (Table 5). Increases in temperature, water vapor and lightning NO_x enhance OH concentrations, and reduce τ_{CH_4} in the model. We note that the evolution of temperature is very similar in the RCP2.6 and RCP4.5* simulations (Fig. 3a), as more warming from increasing CO_2 concentrations in RCP4.5* offsets the aerosol cooling, which has been reduced dramatically (i.e., a warming effect) as sulfate aerosols are considerably decreased in RCP2.6 (e.g. Fig. 4d). Around 2035,

Climate versus emission drivers of methane lifetime

J. G. John et al.

Title Page

Abstract	Introduction
Conclusions	References
Tables	Figures

◄◄	►►
◄	►
Back	Close

Full Screen / Esc

Printer-friendly Version

Interactive Discussion

the temperatures in RCP4.5 separate from RCP4.5*, and by 2100 are warmer by 1.1 K, illustrating that decreasing aerosols can accelerate warming (e.g. Levy et al., 2008; Raes and Seinfeld, 2009; Makkonen et al., 2012). In addition, the decreases in CH_4 and CO further reinforce the climate-driven decrease in τ_{CH_4} in RCP4.5 (Table 5).

In the RCP6.0 scenario, the tropospheric lifetime of methane also decreases, by 5.2 % from 2006–2025 to 2081–2100 (Table 5). Although the temperature, water vapor, and lightning NO_x increases are about 2.5 times greater than in RCP2.6, and both RCP2.6 and RCP6.0 have similar (∼45 %) reductions in NO emissions, there is a smaller decrease in CO emissions in RCP6.0 (18 % vs. 31 %), and the total CH_4 burden increases in RCP6.0 (Table 5), leading to an overall reduction in OH, and a longer average τ_{CH_4} than in RCP2.6 (8.44 vs. 7.72 yr in Table 4). OH decreases from 2006 to the mid 2060s and then rises fairly rapidly until 2100 (Fig. 3b). The latter part of this simulation resembles the last quarter century of WMGGO3 in the CM3 model, in so far as rising temperatures and increased OH (from increasing water vapor, lightning NO_x and photolysis), contribute to a steady decline in τ_{CH_4}.

RCP8.5 is the most extreme warming scenario, with lower tropospheric temperatures warming by 4.5 K from 2006 to 2100 in CM3 (Fig. 3a, Table 5). Despite the increasing temperature (Fig. 3a), which our previous analysis indicates should shorten the τ_{CH_4}, the tropospheric methane lifetime increases, from 8.24 yr in 2006–2025 to 8.73 yr in 2081–2100, with a peak value of 8.91 yr in 2062 (Fig. 1). This increase in lifetime is due to a decrease in OH beginning after 2035, with an overall 14.8 % reduction by the end of the century (Fig. 3b, Table 5). The near doubling of CH_4 abundance by 2100 (Table 5) depletes OH and leads to a positive feedback on the climate system, as concentrations of CH_4 increase further (Prather, 1994). The rise in anthropogenic CH_4 outweighs the climate-driven changes which act to shorten the methane lifetime (Table 5, Fig. 3a, 4a, b, 5a), viz.: rising temperature, water vapor, lightning NO_x. It is interesting to note however that τ_{CH_4} does not keep increasing in a "runaway" effect.

Title Page

Abstract | Introduction

Conclusions | References

Tables | Figures

◄ | ►◄

◄ | ►

Back | Close

Full Screen / Esc

Printer-friendly Version

Interactive Discussion

6   Conclusions

Improved understanding of feedbacks between CH_4 abundances and the climate system are important as they impact not only climate, but also the environment and human health. The relatively short lifetime of methane makes it a suitable candidate for mitigation efforts, as reducing CH_4 emissions decreases radiative forcing and improves air quality (e.g. Fiore et al., 2002; Shindell et al., 2012). Understanding the processes driving the trends and variability in methane lifetime is a crucial step to accurately projecting its future evolution.

We used a suite of CM3 model simulations to evaluate the role of climate and emissions in determining methane lifetime and to pinpoint key drivers from the preindustrial period to the end of the 21st century. Over the historical period, the methane lifetime increases by 5 % overall due to anthropogenic emission increases in CH_4. There are also indications of climatically-driven intervals, e.g. after volcanic events when cooling by aerosols cause the methane lifetime to rise (e.g. HIST in Fig. 1, 3a), or when the effects of increasing temperatures and water vapor create a negative feedback on climate, driving lifetimes down, which in turn decreases the amount of CH_4 in the atmosphere and reduces climate forcing (e.g. WMGGO3 after 1985). During the late 20th century, τ_{CH_4} decreases steadily as rapid warming occurs, and the observed leveling off in atmospheric CH_4 during that time could partially reflect climate-driven influences on the methane sink. Consistent with other model studies, we find a small positive OH trend in recent decades ($0.07\,\%\,\mathrm{yr}^{-1}$ from 1979–1993), which notably conflict with observationally-constrained estimates (Montzka et al., 2011) and merit further study. In particular, process-based approaches, including new global scale satellite observations (e.g. Bloom et al., 2010 for wetlands) should help to elucidate the mechanisms determining atmospheric abundances of methane and OH. Reducing the uncertainty in the contemporary global methane budget would help build confidence in future projections of the CH_4 response to climate change.

Printer-friendly Version

Interactive Discussion

Relative to the simulated historical change (+5 %), the evolution of methane lifetime spans a fairly wide range over the next century, with τ_{CH_4} decreasing overall in RCP2.6, RCP4.5 and RCP6.0 (by 5 to 13 %), but increasing by 4.3 % in RCP8.5 with sharp increases in CH_4 outweighing the extreme warming in this scenario. In a simulation in which only greenhouse gases evolve following the RCP4.5 pathway (RCP4.5*), rising temperatures and enhanced OH shorten τ_{CH_4}. Decreases in aerosol, CO and CH_4 in the full RCP4.5 scenario augment these climate-driven changes to further decrease τ_{CH_4}. We also find positive feedbacks on the climate system; in RCP8.5, the additional CH_4 and other emission changes increase the methane lifetime (despite the tendency of warmer climate to reduce τ_{CH_4}), and amplify climate forcing. There was no tipping point in this scenario, however, as τ_{CH_4} begins to decline by the end of the 21st century. Climate and thereby τ_{CH_4} is sensitive to the representation of the aerosol indirect effect in the CM3 model and represents a major source of uncertainty.

Ongoing efforts such as the Atmospheric Chemistry and Climate Model Intercomparison Project (ACCMIP), provide opportunities to further explore and evaluate the role of climate versus emission-driven changes in determining the trends and variability in the lifetime of methane. Our results offer a benchmark for future analyses of methane lifetime in chemistry-climate models, such as those participating in the ongoing Atmospheric Chemistry and Climate Model Intercomparison Project. Emphasis is particularly needed on the roles of lightning NO_x and photolysis on the methane sink, as well as climate-sensitive methane sources, in order to account fully for all of the competing factors which determine the atmospheric methane lifetime.

References

Allan, W., Lowe, D. C., Gomez, A. J., Struthers, H., and Brailsford, G. W.: Interannual variation of ^{13}C in tropospheric methane: implications for a possible atomic chlorine sink in the marine boundary layer, J. Geophys. Res., 110, D11306, doi:10.1029/2004JD005650, 2005.

Arneth, A., Harrison, S. P., Zaehle, S., Tsigaridis, K., Menon, S., Bartlein, P. J., Feichter, J., Korhola, A., Kulmala, M., O'Donnell, D., Schurgers, G., Sorvari, S., and Vesala, T.: Terrestrial biogeochemical feedbacks in the climate system, Nat. Geosci., 3, 525–532, doi:10.1038/ngeo905, 2010.

Austin, J. and Wilson, R. J.: Ensemble simulations of the decline and recovery of stratospheric ozone, J. Geophys. Res., 111, D16314, doi:10.1029/2005JD006907, 2006.

Aydin, M., Verhulst, K. R., Saltzmann, E. S., Battle, M. O., Montzka, S. A., Blake, D. R., Tang, Q., and Prather, M. J.: Recent decreases in fossil-fuel emissions of ethane and methane derived from firn air, Nature, 476, 198–201, doi:10.1038/nature10352, 2011.

Bekki, S. and Law, K. S.: Sensitivity of the atmospheric CH_4 growth rate to global temperature changes observed from 1980 to 1992, Tellus B, 49, 409–416, 1997.

Berntsen, T. K., Isaksen, I. S. A., Myhre, G., Fuglestvedt, J. S., Stordal, F., Larsen, T. A., Freckleton, R. S., and Shine, K. P.: Effects of anthropogenic emissions on tropospheric ozone and its radiative forcing, J. Geophys. Res., 102, 28101–28126, doi:10.1029/97JD02226, 1997.

Bloom, A. A., Palmer, P. I., Fraser, A., Reay, D. S., and Frankenberg, C.: Large-scale controls of methanogenesis inferred from methane and gravity spaceborne data, Science, 327, 322–325, 2010.

Bousquet, P., Hauglustaine, D. A., Peylin, P., Carouge, C., and Ciais, P.: Two decades of OH variability as inferred by an inversion of atmospheric transport and chemistry of methyl chloroform, Atmos. Chem. Phys., 5, 2635–2656, doi:10.5194/acp-5-2635-2005, 2005.

Bousquet, P., Ciais, P., Miller, J. B., Dlugokencky, E. J., Hauglustaine, D. A., Prigent, C., Van der Werf, G. R., Peylin, P., Brunke, E. G., Carouge, C., Langenfels, R. L., Lathiere, J., Papa, F., Ramonet, M., Schmidt, M., Steele, L. P., Tyler, S. C., and White, J.: Contribution of anthropogenic and natural sources to atmospheric methane variability, Nature, 443, 439–443, 2006.

Brasseur, G. J., Kiehl, T., Muller, J. F., Schneider, T., Granier, C., Tie, X. X., and Hauglustaine, D.: Past and future changes in global tropospheric ozone: impact on radiative forcing, Geophys. Res. Lett., 25, 3807–3810, 1998.

Climate versus emission drivers of methane lifetime

J. G. John et al.

Crutzen, P. J. and Zimmermann, P. H.: The changing photochemistry of the troposphere, Tellus B, 43, 136–151, 1991.

Crutzen, P. J., Lawrence, M. G., and Pöschl, U.: On the background photochemistry of tropospheric ozone, Tellus, 51, 123–146, 1999.

Dalsøren, S. B. and Isaksen, I. S. A.: CTM study of changes in tropospheric hydroxyl distribution 1990–2001 and its impact on methane, Geophys. Res. Lett., 33, L23811, doi:10.1029/2006GL027295, 2006.

Denman, K. L., Brasseur, G., Chidthaisong, A., Ciais, P., Cox, P. M., Dickenson, R. E., Hauglustaine, D., Heinze, C., Holland, E., Jacob, D. J., Lohmann, U., Ramachandran, S., da Silva Dias, P. L., Wofsy, S. C., and Zhang, X.: Couplings between changes in the climate system and biogeochemistry, in: Climate Change 2007: The Physical Science Basis. Contribution of Working Group I to the Fourth Assessment Report of the Intergovernmental Panel on Climate Change, edited by: Solomon, S., Qin, D., Manning, M., Chen, Z., Marquis, M., Averyt, K. B., Tignor, M., and Miller, H. L., Cambridge University Press, Cambridge, 2007.

Dentener, F., Peters, W., Krol, M., Van Weele, M., Bergamaschi, P., and Lelieveld, J.: Interannual variability and trend of CH_4 lifetime as a measure for OH changes in the 1979–1993 time period, J. Geophys. Res., 108, 4442, doi:10.1029/2002JD002916, 2003.

Dlugokencky, E. J., Masarie, K. A., Lang, P. M., and Tans, P. P.: Continuing decline in the growth rate of the atmospheric methane burden, Nature, 393, 447–450, 1998.

Dlugokencky, E. J., Houweling, S., Bruhwiler, L., Masarie, K. A., Lang, P. M., Miller, J. B., and Tans, P. P.: Atmospheric methane levels off: temporary pause or a new steady-state?, Geophys. Res. Lett., 30, 1992, doi:10.1029/2003GL018126, 2003.

Donner, L. J., Wyman, B. L., Hemler, R. S., Horowitz, L. W., Ming, Y., Zhoa, M., Golaz, J.-C., Ginoux, P., Lin, S.-J., Schwarkopf, M. D., Austin, J., Alaka, G., Cooke, W. F., Delworth, T. L., Freidenreich, S. M., Gordon, C. T., Griffies, S. M., Held, I. M., Hurlin, W. J., Klein, S. A., Knutson, T. R., Langenhorst, A. R., Lee, H.-C., Lin, Y., Magi, B. I., Malyshev, S. L., Milly, P. C. D., Naik, V., Nath, M. J., Pincus, R., Ploshay, J. J., Ramaswamy, V., Seman, C. J., Shevliakova, E., Sirutis, J. J., Stern, W. F., Stouffer, R. J., Stouffer, R. J., Wilson, R. J., Winton, M., Wittenberg, A. T., and Zeng, F.: The dynamical core, physical parameterizations, and basic simulation characteristics of the atmospheric component AM3 of the GFDL Global Coupled Model CM3, J. Climate, 24, 3484–3519, 2011.

Fiore, A. M., Jacob, D. J., Field, B. D., Streets, D. G., Fernandes, S. D., and Jang, C.: Linking ozone pollution and climate change: the case for controlling methane, Geophys. Res. Lett., 29, 1919, doi:10.1029/2002GL015601, 2002.

Fiore, A. M., Horowitz, L. W., Dlugokencky, E. J., and West, J. J.: Impact of meteorology and emissions on methane trends, 1990–2004, Geophys. Res. Lett., 33, L12809, doi:10.1029/2006GL026199, 2006.

Fiore, A. M., West, J. J., Horowitz, L. W., Naik, V., and Schwarzkopf, M. D.: Characterizing the tropospheric ozone response to methane emission controls and the benefits to climate and air quality, J. Geophys. Res., 113, D08307, doi:10.1029/2007JD009162, 2008.

Flückiger, J., Monnin, E., Stauffer, B., Schwander, J. and Stocker, T. F.: High-resolution holocene N_2O ice core record and its relationship with CH_4 and CO_2, Global Biogeochem. Cy., 16, 1010, doi:10.1029/2001GB001417, 2002.

Forster, P., Ramaswamy, V., Artaxo, P., Berntsen, T., Betts, R., Fahey, D. W., Haywood, J., Lean, J., Lowe, D. C., Myhre, G., Nganga, J., Prinn, R., Raga, G., Schulz, M., and Van Dorland, R.: Changes in atmospheric constituents and in radiative forcing, in: Climate Change 2007: The Physical Science Basis. Contribution of Working Group I to the Fourth Assessment Report of the Intergovernmental Panel on Climate Change, edited by: Solomon, S., Qin, D., Manning, M., Chen, Z., Marquis, M., Averyt, K. B., Tignor, M., and Miller, H. L., Cambridge University Press, Cambridge, UK and New York, NY, USA, 2007.

Grenfell, J. L., Shindell, D. T., Koch, D., and Rind, D.: Chemistry-climate interactions in the Goddard Institute general circulation model. 2. New insights into modeling the pre-industrial atmosphere, J. Geophys. Res., 106, 33435–33451, 2001.

Griffies, S. M, Winton, M., Donner, L. J., Horowitz, L. W., Downes, S. M., Farneti, R., Gnanadesikan, A., Hurlin, W. J., Lee, H.-C., Liang, Z., Palter, J. B., Samuels, B. L., Wittenberg, A. T., Wyman, B. L., Yin, J., and Zadeh, N.: The GFDL CM3 coupled climate model: characteristics of the ocean and sea ice simulations, J. Climate, 24, 3520–3544, 2011.

Hamilton, K. and Fan, S.-M.: Effects of the stratospheric quasi-biennial oscillation on long-lived greenhouse gases in the atmosphere, J. Geophys. Res., 105, 20581–20587, 2000.

Hauglustaine, D. A. and Brasseur, G. P.: Evolution of tropospheric ozone under anthropogenic activities and associated radiative forcing of climate, J. Geophys. Res., 106, 32337–32360, doi:10.1029/2001JD900175, 2001.

Title Page

Abstract | Introduction

Conclusions | References

Tables | Figures

◄ | ►

◄ | ►

Back | Close

Full Screen / Esc

Printer-friendly Version

Interactive Discussion

Hodson, E. L., Poulter, B., Zimmermann, N. E., Prigent, C., and Kaplan, J. O.: The El Niño–Southern Oscillation and wetland methane interannual variability, Geophys. Res. Lett., 38, L08810, doi:10.1029/2011GL046861, 2011.

Horowitz, L. W.: Past, present, and future concentrations of tropospheric ozone and aerosols: methodology, ozone evaluation and sensitivity to aerosol wet removal, J. Geophys. Res., 111, D22211, doi:10.1029/2005JD006937, 2006.

Horowitz, L. W., Walters, S., Mauzerall, D. L., Emmons, L. K., Rasch, P. J., Granier, C., Tie, X., Lamarque, J.-F., Schultz, M. G., Tyndall, G. S., Orlando, J. J., and Brasseur, G. P.: A global simulation of tropospheric ozone and related tracers: description and evaluation of MOZART, version 2, J. Geophys. Res., 108, 4784, doi:10.1029/2002JD002853, 2003.

Johnson, C. E., Stevenson, D. S., Collins, W. J., and Derwent, R. G.: Interannual variability in methane growth rate simulated with a coupled ocean-atmosphere chemistry model, Geophys. Res. Lett., 29, 1903, doi:10.1029/2002GL015269, 2002.

Kai, F. M., Tyler, S. C., Randerson, J. T., and Blake, D. R.: Reduced methane growth rate explained by decreased Northern Hemisphere microbial sources, Nature, 476, 194–197, 2011.

Karlsdóttir, S. and Isaksen, I. S. A.: Changing methane lifetime: possible cause for reduced growth, Geophys. Res. Lett., 27, 93–96, 2000.

Krol, M., van Leeuwen, P. J., and Lelieveld, J.: Global OH trend inferred from methyl-chloroform measurements, J. Geophys. Res., 103, 10697–10711, 1998.

Lamarque, J.-F., Hess, P., Emmons, L., Buja, L., Washington, W., and Granier, C.: Tropospheric ozone evolution between 1890 and 1990, J. Geophys. Res., 110, D08304, doi:10.1029/2004JD005537, 2005.

Lamarque, J.-F., Bond, T. C., Eyring, V., Granier, C., Heil, A., Klimont, Z., Lee, D., Liousse, C., Mieville, A., Owen, B., Schultz, M. G., Shindell, D., Smith, S. J., Stehfest, E., Van Aardenne, J., Cooper, O. R., Kainuma, M., Mahowald, N., McConnell, J. R., Naik, V., Riahi, K., and van Vuuren, D. P.: Historical (1850–2000) gridded anthropogenic and biomass burning emissions of reactive gases and aerosols: methodology and application, Atmos. Chem. Phys., 10, 7017–7039, doi:10.5194/acp-10-7017-2010, 2010.

Law, K. S. and Nisbet, E. G.: Sensitivity of the methane growth rate to changes in methane emissions from natural gas and coal, J. Geophys. Res., 101, 14387–14397, 1996.

Lawrence, M. G., Jöckel, P., and von Kuhlmann, R.: What does the global mean OH concentration tell us?, Atmos. Chem. Phys., 1, 37–49, doi:10.5194/acp-1-37-2001, 2001.

Climate versus emission drivers of methane lifetime

J. G. John et al.

Lelieveld, J., Crutzen, P. J., and Dentener, F. J.: Changing concentration, lifetime and climate forcing of atmospheric methane, Tellus B, 50, 128–150, 1998.

Lelieveld, J., Peters, W., Dentener, F. J., and Krol, M. C.: Stability of tropospheric hydroxyl chemistry, J. Geophys. Res., 107, 4715, doi:10.1029/2002JD002272, 2002.

Levy, H.: Normal atmosphere: large radical and formaldehyde concentrations predicted, Science, 173, 141–143, 1971.

Levy, H., Moxim, W. J., and Kasibhatla, P. S.: A global three-dimensional time-dependent lightning source of tropospheric NO_x, J. Geophys. Res., 101, 22911–22922, 1996.

Levy, H., Schwarzkopf, M. D., Horowitz, L., Ramaswamy, V., and Findell, K. L.: Strong sensitivity of late 21st century climate to projected changes in short-lived air pollutants, J. Geophys. Res., 113, D06102, doi:10.1029/2007JD009176, 2008.

Logan, J. A., Prather, M. J., Wofsy, S. C., and McElroy, M. B.: Tropospheric chemistry: a global perspective, J. Geophys. Res., 86, 7210–7254, 1981.

Makkonen, R., Asmi, A., Kerminen, V.-M., Boy, M., Arneth, A., Hari, P., and Kulmala, M.: Air pollution control and decreasing new particle formation lead to strong climate warming, Atmos. Chem. Phys., 12, 1515–1524, doi:10.5194/acp-12-1515-2012, 2012.

Martinerie, P., Brasseur, G. P., and Granier, C.: The chemical composition of ancient atmospheres: a model study constrained by ice core data, J. Geophys. Res., 100, 14291–14304, 1995.

Masui, T., Matsumoto, K., Hijioka, Y., Kinoshita, T., Nozawa, T., Ishiwatari, S., Kato, E., Shukla, P. R., Yamagata, Y., and Kainuma, M.: An emission pathway for stabilization at $6 \, W \, m^{-2}$ radiative forcing, Climatic Change, 109, 59–76, doi:10.1007/s10584-011-0150-5, 2011.

Meinshausen, M., Smith, S. J., Calvin, K., Daniel, J. S., Kainuma M. L. T., Lamarque, J.-F., Matsumoto, K., Montzka, S. A., Raper, S. C. B., Riahi, K., Thomson, A., Velders, G. J. M., and van Vuuren, D. P. P.: The RCP greenhouse gas concentrations and their extensions from 1765 to 2300, Climatic Change, 109, 213–241, doi:10.1007/s10584-011-0156-z, 2011.

Mickley, L. J., Murti, P. P., Jacob, D. J., Logan, J. A., Koch, D. M., and Rind, D.: Radiative forcing from tropospheric ozone calculated with a unified chemistry climate model, J. Geophys. Res., 104, 30153–30172, 1999.

Montzka, S. A., Krol, M., Dlugokencky, E., Hall, B., Jöckel, P., and Lelieveld, J.: Small interannual variability of global atmospheric hydroxyl, Science, 331, 67–69, doi:10.1126/science.1197640, 2011.

Moss, R. H., Edmonds, J. A., Hibbard, K. A., Manning, M. R., Rose, S. K., van Vuuren, D. P., Carter, T. R., Emori, S., Kainuma, M., Kram, T., Meehl, G. A., Mitchell, J. F. B., Nakicenovic, N., Riahi, K., Smith, S. J., Stouffer, R. J., Thomson, A. M., Weyant, J. P., and Wilbanks, T. J.: The next generation of scenarios for climate change research and assessment, Nature, 463, 747–756, doi:10.1038/nature08823, 2010.

Naik, V., Horowitz, L. W., Fiore, A. M., Ginoux, P., Mao, J., Aghedo, A., and Levy, H.: Preindustrial to present day impact of changes in short-lived pollutant emissions on atmospheric composition and climate forcing, J. Geophys. Res., submitted, 2012.

Osborn T. J. and Wigley, T. M. L.: A simple model for estimating methane concentration and lifetime variations, Clim. Dynam., 9, 181–193, 1994.

Prather, M. J.: Lifetimes and eigenstates in atmospheric chemistry, Geophys. Res. Lett., 21, 801–804, 1994.

Prather, M. J. and Spivakovsky, C. M.: Tropospheric OH and the lifetimes of hydrochlorofluorocarbons, J. Geophys. Res., 95, 18723–18729, 1990.

Prather, M., Gauss, M., Berntsen, T., Isaksen, I., Sundet, J., Bey, I., Brasseur, G., Dentener, F., Derwent, R., Stevenson, D., Grenfell, L., Hauglustaine, D., Horowitz, L., Jacob, D., Mickley, L., Lawrence, M. G., von Kuhlmann, R., Muller, J.-F., Pitari, G., Rogers, H., Johnson, M., Pyle, J., Law, K., van Weele, M., and Wild, O.: Fresh air in the 21st century?, Geophys., Res. Lett., 30, 1100, doi:10.1029/2002GL016285, 2003.

Price, C., Penner, J., and Prather M.: NO_x from lightning. 1. Global distribution based on lightning physics, J. Geophys. Res., 102, 5929–5941, 1997.

Prinn, R. G., Weiss, R. F., Miller, B. R., Huang, J., Alyea F. N., Cunnold, D. M., Fraser, P. J., Hartley, D. E., and Simmonds, P. G: Atmospheric trends and lifetime of CH_3CCl_3 and global OH concentrations, Science, 269, 187–192, 1995.

Prinn, R. G., Huang, J., Weiss, R. F., Cunnold, D. M., Fraser, P. J., Simmonds, P. G., McCulloch, A., Harth, C., Salameh, P., O'Doherty, S., Wang, R. H. J., Porter, L., and Miller, B. R.: Evidence for substantial variations of atmospheric hydroxyl radicals over the past two decades, Science, 292, 1882–1888, 2001.

Prinn, R. G., Huang, J., Weiss, R. F., Cunnold, D. M., Fraser, P. J., Simmonds, P. G., McCulloch, A., Harth, C., Reimann, S., Salameh, P., O'Doherty, S., Wang, R. H. J., Porter, L. W., Miller, B. R., and Krummel, P. B.: Evidence for variability of atmospheric hydroxyl radicals over the past quarter century, Geophys. Res. Lett., 32, L07809, doi:10.1029/2004GL022228, 2005.

Climate versus emission drivers of methane lifetime

J. G. John et al.

Title Page

Abstract	Introduction
Conclusions	References
Tables	Figures

◀ ▶

◀ ▶

Back | Close

Full Screen / Esc

Printer-friendly Version

Interactive Discussion

Raes, F. and Seinfeld, J. H.: New directions: climate change and air pollution abatement: a bumpy road, Atmos. Environ., 43, 5132–5133, doi:10.1016/j.atmosenv.2009.06.001, 2009.

Riahi, K., Rao, S., Krey, V., Cho, C., Chirkov, V., Fischer, G., Kindermann G., Nakicenovic, N., and Rafaj, P.: RCP 8.5 – a scenario of comparatively high greenhouse gas emissions, Climatic Change, 109, 33–57, doi 10.1007/s10584-011-0149-y, 2011.

Rigby, M., Prinn, R. G., Fraser, P. J., Simmonds, P. G., Langenfelds, R. L., Huang, J., Cunnold, D. M., Steele, L. P., Krummel, P. B., Weiss, R. F., O'Doherty, S., Salameh, P. K., Wang, H. J., Harth, C. M., Mühle, J., and Porter, L. W.: Renewed growth of atmospheric methane, Geophys. Res. Lett., 35, L22805, doi:10.1029/2008GL036037, 2008.

Roelofs, G. J., Lelieveld, J., and van Dorland, R.: A three-dimensional chemistry-general circulation model simulation of anthropogenically derived ozone in the troposphere and its radiative climate forcing, J. Geophys. Res., 102, 23389–23401, 1997.

Sander, S. P., Friedl, R. R., Golden, D. M., Kurylo, M. J., Huie, R. E., Orkin, V. L., Moortgat, G. K., Wine, P. H., Ravishankara, A. R., Kolb, C. E., Molina, M. J., Finlayson-Pitts, B. J., Huie, R. E., and Orkin, V. L.: Chemical Kinetics and Photochemical Data for Use in Atmospheric Studies, Evaluation Number 15, JPL Publications 06-2, Jet Propulsion Laboratory, Pasadena, CA, USA, 2006.

Shevliakova, E., Pacala S. W., Malyshev S., Hurtt G. C., Milly P. C. D., Caspersen J. P., Sentman L. T., Fisk J. P., Wirth C., and Crevoisier C.: Carbon cycling under 300 yr of land use change: importance of the secondary vegetation sink, Global Biogeochem. Cy., 23, GB2022, doi:10.1029/2007GB003176, 2009.

Shindell, D. T., Grenfell, J. L., Rind, D., Grewe, V., and Price, C.: Chemistry-climate interactions in the Goddard Institute for Space Studies general circulation model 1. Tropospheric chemistry model description and evaluation, J. Geophys. Res., 106, 8047–8075, 2001.

Shindell, D. T., Faluvegi, G., Bell, N., and Schmidt, G. A.: An emissions-based view of climate forcing by methane and tropospheric ozone, Geophys. Res. Lett., 32, L04803, doi:10.1029/2004GL021900, 2005.

Shindell, D. T., Faluvegi, G., Unger, N., Aguilar, E., Schmidt, G. A., Koch, D. M., Bauer, S. E., and Miller, R. L.: Simulations of preindustrial, present-day, and 2100 conditions in the NASA GISS composition and climate model G-PUCCINI, Atmos. Chem. Phys., 6, 4427–4459, doi:10.5194/acp-6-4427-2006, 2006.

Shindell, D., Kuylenstierna, J. C. I., Vignati, E., Van Dingenen, R., Amann, M., Klimont, Z., Anenberg, S. C., Muller, N. Z., Janssens-Maenhout, G., Raes, F., Schwartz, J., Faluvegi, G.,

Climate versus emission drivers of methane lifetime

J. G. John et al.

Title Page

Abstract | Introduction

Conclusions | References

Tables | Figures

◄◄ | ►►

◄ | ►

Back | Close

Full Screen / Esc

Printer-friendly Version

Interactive Discussion

Pozzoli, L., Kupiainen, K., Hoglund-Isaksson, L., Emberson, L., Streets, D., Ramanathan, V., Hicks, K., Oanh, N. T. K., Milly, G., Williams, M., Demkine, V., and Fowler, D.: Simultaneously mitigating near-term climate change and improving human health and food security, Science, 335, 183–189, 2012.

Sofen, E. D., Alexander, B., and Kunasek, S. A.: The impact of anthropogenic emissions on atmospheric sulfate production pathways, oxidants, and ice core $\Delta^{17}O(SO_4^{2-})$, Atmos. Chem. Phys., 11, 3565–3578, doi:10.5194/acp-11-3565-2011, 2011.

Søvde, O. A., Hoyle, C. R., Myhre, G., and Isaksen, I. S. A.: The HNO_3 forming branch of the HO_2 + NO reaction: pre-industrial-to-present trends in atmospheric species and radiative forcings, Atmos. Chem. Phys., 11, 8929–8943, doi:10.5194/acp-11-8929-2011, 2011.

Spivakovsky, C. M., Logan, J. A., Montzka, S. A., Balkanski, Y. J., Foreman-Fowler, M., Jones, D. B. A., Horowitz, L. W., Fusco, A. C., Brenninkmeijer, C. A. M., Prather, M. J., Wofsy, S. C., and McElroy, M. B., Three-dimensional climatological distribution of tropospheric OH: update and evaluation, J. Geophys. Res., 105, 8931–8980, 2000.

Staffelbach, T., Neftel, A., Stauffer, B., and Jacob, D.: A record of the atmospheric methane sink from formaldehyde in polar ice cores, Nature, 349, 603–605, doi:10.1038/349603a0, 1991.

Stevenson, D. S., Dentener, F. J., Schultz, M. G., Ellingsen, K., van Noije, T. P. C., Wild, O., Zeng, G., Amann, M., Atherton, C. S., Bell, N., Bergmann, D. J., Bey, I., Butler, T., Cofala, J., Collins, W. J., Derwent, R. G., Doherty, R. M., Drevet, J., Eskes, H. J., Fiore, A. M., Gauss, M., Hauglustaine, D. A., Horowitz, L. W., Isaksen, I. S. A., Krol, M. C., Lamarque, J., Lawrence, M. G., Montanaro, V., Müller, J., Pitari, G., Prather, M. J., Pyle, J. A., Rast, S., Rodriguez, J. M., Sanderson, M. G., Savage, N. H., Shindell, D. T., Strahan, S. E., Sudo, K., and Szopa, S.: Multimodel ensemble simulations of present-day and near-future tropospheric ozone, J. Geophys. Res.-Atmos., 111, D08301, doi:10.1029/2005JD006338, 2006.

Taylor, K. E., Stouffer, R. J., and Meehl, G. A.: An overview of CMIP5 and the experiment design, B. Am. Meteorol. Soc., 93, 485–498, doi:10.1175/BAMS-D-11-00094.1, 2012.

Thompson, A. M., Chappellaz, J. A., Fung, I. Y., and Kucsera, T. L.: The atmospheric CH_4 increase since the Last Glacial Maximum. II – Interactions with oxidants, Tellus, 45, 242–257, doi:10.1034/j.1600-0889.1993.t01-2-00003.x, 1993.

Thomson, A. M., Calvin, K. V., Smith, S. J., Kyle, G. P., Volke, A., Patel, P., Delgado-Arias, S., Bond-Lamberty, B., Wise, M. A., Clarke, L. E., and Edmonds, J. A.: RCP4.5: a pathway for stabilization of radiative forcing by 2100, Climatic Change, 109, 77–94, doi:10.1007/s10584-011-0151-4, 2011.

Unger, N., Menon, S., Koch, D. M., and Shindell, D. T.: Impacts of aerosol-cloud interactions on past and future changes in tropospheric composition, Atmos. Chem. Phys., 9, 4115–4129, doi:10.5194/acp-9-4115-2009, 2009.

van Vuuren, D., Edmonds, J., Kainuma, M., Riahi, K., Thomson, A., Hibbard, K., Hurtt, G., Kram, T., Krey, V., Lamarque, J.-F., Masui, T., Meinshausen, M., Nakicenovic, N., Smith, S., and Rose, S.: The representative concentration pathways: an overview, Climatic Change, 109, 5–31, doi:10.1007/s10584-011-0148-z, 2011a.

van Vuuren, D., Stehfest, E., den Elzen, M., Kram, T., van Vliet, J., Deetman, S., Isaac, M., Klein Goldewijk, K., Hof, A., Mendoza Beltran, A., Oostenrijk, R., and van Ruijven, B.: RCP2.6: exploring the possibility to keep global mean temperature increase below 2˚C, Climatic Change, 109, 95–116, doi:10.1007/s10584-011-0152-3, 2011b.

Wang, J. S., Logan, J. A., McElroy, M. B., Duncan, B. N., Megretskaia, I. A., and Yantosca, R. M.: A 3-D model analysis of the slowdown and interannual variability in the methane growth rate from 1988–1997, Global Biogeochem. Cy., 18, GB3011, doi:10.1029/2003GB002180, 2004.

Wang, Y. and Jacob, J. D.: Anthropogenic forcing on tropospheric ozone and OH since preindustrial times, J. Geophys. Res., 103, 31123–31135, 1998.

Warwick, N. J., Bekki, S., Law, K. S., Nisbet, E. G., and Pyle, J. A.: The impact of meteorology on the interannual growth rate of atmospheric methane, Geophys. Res. Lett., 29, 1947, doi:10.1029/2002GL015282, 2002.

West, J. J., Fiore, A. M., Horowitz, L. W., and Mauzerall, D. L.: Global health benefits of mitigating ozone pollution with methane emission controls, P. Natl. Acad. Sci. USA, 103, 3988–3993, doi:10.1073/pnas.0600201103, 2006.

Title Page

Abstract | Introduction

Conclusions | References

Tables | Figures

◄ | ►

◄ | ►

Back | Close

Full Screen / Esc

Printer-friendly Version

Interactive Discussion

Table 1. Percent changes in methane lifetime and OH compiled from literature. Note that the definition of methane lifetime is not necessarily the same in references below.

Reference	% Change in methane lifetime since preindustrial	Method
Osborn and Wigley (1994)[a]	+15 % to +34 %	parameterized model
Martinerie et al. (1995)[a]	−14.1 %	2-D model
Lelieveld et al. (1998)[b]	+27.4 %	3-D model
Unger et al. (2009)[a]	+13 %, +11.6 %	3-D model (with, w/o aerosol-cloud interactions)
Søvde et al. (2011)[a]	+4.6 %, +4.0 %	3-D model (with, w/o HO_2 +NO → HNO_3)

Reference	% Change in OH since preindustrial	Method
Staffelbach et al. (1991)	−30 %	ice core measurements of CH_2O
Crutzen and Zimmerman (1991)	−10 % to −20 %	3-D model
Thompson et al. (1993)	−20 %	Multi 1-D model
Martinerie et al. (1995)	+6 %	2-D model
Berntsen et al. (1997)	+6.8 %	3-D model
Roelofs et al. (1997)	−22 %	3-D model
Brasseur et al. (1998)	−17 %	3-D model
Wang and Jacob (1998)	−9 %	3-D model
Mickley et al. (1999)	−16 %	3-D model
Grenfell et al. (2001)	−4 %	3-D model without non-methane hydrocarbon (NMHC)
Hauglustaine and Brasseur (2001)	−33 %	3-D model
Shindell et al. (2001)	−5.9 %	3-D model
Lelieveld et al. (2002)	−5 %	3-D model
Lamarque et al. (2005)	−8 %	3-D model
Shindell et al. (2006)	−16 %	3-D model
Sofen et al. (2011)	−10 %	3-D model

[a] Tropospheric lifetime with respect to OH or chemical lifetime.
[b] Total lifetime (includes all loss processes).

Title Page

Abstract | Introduction

Conclusions | References

Tables | Figures

◄ | ►►

◄ | ►

Back | Close

Full Screen / Esc

Printer-friendly Version

Interactive Discussion

Title Page

Abstract | Introduction

Conclusions | References

Tables | Figures

◄◄ | ►►

◄ | ►

Back | Close

Full Screen / Esc

Printer-friendly Version

Interactive Discussion

Table 2. Summary of major drivers of methane and OH trends, growth rates and interannual variability (IAV) from previous studies.

Reference	Time Period	Major drivers of CH_4 trends, growth rates and IAV	Method
Law and Nisbet (1996)	1980–1994	decline in CH_4 growth rate from 1989–1992 due to reductions in fossil fuel emissions from former Soviet Union	2-D model
Bekki and Law (1997)	1980–1992	decline in CH_4 growth rate due to temperature dependency of rate constant and CH_4 emissions from wetlands	2-D model
Dlugokencky et al. (1998)	1984–1996	decrease in CH_4 growth rate due to approach to steady state	Observations/Analysis
Hamilton and Fan (2000)	1980–1999	stratospheric quasi-biennial oscillation contributes to CH_4 growth rate	3-D model
Karlsdóttir and Isaksen (2000)	1980–1996	increasing anthropogenic emissions in SE Asia	3-D model
Johnson et al. (2002)	1990–2009	CH_4 interannual variability driven by OH (water vapor)	3-D model
Warwick et al. (2002)	1980–1998	CH_4 interannual variability due to vertical redistribution and transport changes	3-D model
Dlugokencky et al. (2003)	1984–2002	equilibrium/steady state; wetlands	Observations/Analysis
Wang et al. (2004)	1988–1997	decrease in CH_4 growth rate due to reduced anthropogenic emissions, increasing OH	3-D model
Bousquet et al. (2006)	1984–2003	decline in anthropogenic emissions; wetland emissions	Inversion
Fiore et al. (2006)	1990–2004	increasing OH and temperature	3-D model
Aydin et al. (2011)	1980–2000	reduced fossil fuel emissions	Firn air measurements
Hodson et al. (2011)	1950–2005	ENSO variability	Wetland CH_4 model
Kai et al. (2011)	1984–2005	reduced emissions from rice paddies in Asia	Isotopic constraints

Table 2. Continued.

Reference	Time Period	OH trends, growth rates and IAV	Method
Prinn et al. (1995)	1978–1994	OH trend: $0.0 \pm 0.2\,\%\,\mathrm{yr}^{-1}$	Observations/Analysis
Krol et al. (1998)	1978–1993	positive OH trend $(0.46 \pm 0.6\,\%\,\mathrm{yr}^{-1})$ due to stratospheric O_3 depletion, declining CO, increased water vapor and NO_x emissions	3-D model
Karlsdóttir and Isaksen (2000)	1980–1996	positive OH trend $(0.43\,\%\,\mathrm{yr}^{-1})$ due to changes in CO, NO_x and NMHC emissions	3-D model
Prinn et al. (2001)	1978–2000	negative OH trend: $-0.64 \pm 0.60\,\%\,\mathrm{yr}^{-1}$	Observations/Analysis
Dentener et al. (2003)	1979–1993	positive OH trend $(0.24 \pm 0.06\,\%\,\mathrm{yr}^{-1})$ due to changes in water vapor in tropical troposphere	3-D model
Wang et al. (2004)	1988–1997	positive OH trend $(0.64\,\%\,\mathrm{yr}^{-1})$ due to decrease in column O_3	3-D model
Bousquet et al. (2005)	1979–2000	negative OH trend after 1980 $(-0.7 \pm 0.2\,\%\,\mathrm{yr}^{-1})$	Inversion
Dalsøren and Isaksen (2006)	1990–2001	positive OH trend $(0.08\,\%\,\mathrm{yr}^{-1})$ from varying CO, NO_x, NMVOC emissions	3-D model
Montzka et al. (2011)	1998–2007	OH interannual variability: $2.3 \pm 1.5\,\%$	CH_3CCl_3 observations

Table 3. Summary of forcings and emissions used in CM3/CMIP5 simulations. All simulations use dynamic vegetation, except for 1860 CONTROL which uses static vegetation.

Experiment	Solar	Volcanoes	WMGHG (radiation)	WMGHG (chemistry)	Aerosol emission	Ozone Precursors (emission/conc)	LandUse	Radiative and Land CO_2
CONTROL	1860	none	1860	1860	1860	1860	1860	1860
HIST (5 member ensemble)	Historical	Historical	Historical	Historical	Historical	Historical	Historical	Historical
AEROSOL[a] (3 member ensemble)	1860	none	1860	1860	Historical	1860	1860	1860
AEROSOL INDIRECT (3 member ensemble)	1860	none	1860	1860	1860 climatology	1860	1860	1860
ANTHRO (3 member ensemble)	1860	none	Historical	Historical	Historical	Historical	Historical	Historical
NATURAL[b] (3 member ensemble)	Historical	Historical	1860	1860	1860	1860	1860	1860
WMGGO3[c] (3 member ensemble)	1860	none	Historical	Historical	1860	Historical	1860	Historical
RCP2.6	RCP2.6	none	RCP2.6	RCP2.6	RCP2.6	RCP2.6	RCP2.6	RCP2.6
RCP4.5 (3 member ensemble)	RCP4.5	none	RCP4.5	RCP4.5	RCP4.5	RCP4.5	RCP4.5	RCP4.5
RCP4.5*[d] (3 member ensemble)	RCP4.5	none	RCP4.5	RCP4.5; 2005 for CH_4, N_2O, ODS	2005	2005	RCP4.5	RCP4.5
RCP6.0	RCP6.0	none	RCP6.0	RCP6.0	RCP6.0	RCP6.0	RCP6.0	RCP6.0
RCP8.5	RCP8.5	none	RCP8.5	RCP8.5	RCP8.5	RCP8.5	RCP8.5	RCP8.5

[a] AEROSOL: only aerosols, SO_2/BC/OC emissions are time-varying.

[b] NATURAL: GHG for radiation and chemistry fixed at 1860 values. CFCs fixed at 1860 values.

[c] WMGGO3: SO_2 and aerosols held at 1860 values.

[d] RCP4.5*: CH_4, N_2O and ODS for chemistry are fixed at 2005 values. Aerosol and O_3 precursor emissions also fixed to 2005 values.

Table 4. Mean and standard deviation (σ) of annual mean methane lifetime (yr), and correlation coefficient (r) of τ_{CH_4} with global annual mean airmass-weighted OH and temperature (both below 500 hPa), in CM3/CMIP5 simulations. All values are reported over the length of model simulation periods (146 yr for historical, 95 yr for RCPs), except for $\tau_{CH_4\text{-}1986\_2005}$, the methane lifetime over the last 20 yr (1986–2005) of the historical ensemble.

Experiment	τ_{CH_4} Mean $\pm \sigma$ (yr)	$\tau_{CH_4\text{-}1986\_2005}$ Mean $\pm \sigma$ (yr)	$r\_$OH (below 500 hPa)	$r\_$TEMP (below 500 hPa)
HIST	8.63 ± 0.24	8.67 ± 0.16	−0.97	−0.19
AEROSOL	8.50 ± 0.22	8.88 ± 0.04	−0.99	−0.99
AEROSOL INDIRECT	8.52 ± 0.21	8.88 ± 0.04	−0.99	−0.98
ANTHRO	8.44 ± 0.22	8.62 ± 0.08	−0.98	0.25
NATURAL	8.45 ± 0.13	8.48 ± 0.12	−0.98	−0.91
WMGGO3	8.14 ± 0.12	7.88 ± 0.09	−0.07	−0.77
RCP2.6	7.72 ± 0.36		−0.99	−0.92
RCP4.5	7.85 ± 0.40		−0.98	−0.98
RCP4.5*	8.18 ± 0.16		−0.97	−0.99
RCP6.0	8.41 ± 0.21		−0.32	−0.80
RCP8.5	8.61 ± 0.19		−0.90	0.78

Table 5. Percent change of τ_{CH_4}, temperature change (ΔTEMP) in Kelvin, percent change of rate constant (Δk), OH (ΔOH), CH$_4$ (ΔCH$_4$), CO emissions (ΔCOEMIS), surface NO emissions (ΔNOEMIS), lightning NO$_x$ (ΔLNO$_x$), water vapor (ΔH$_2$O), and photolysis (ΔJ(O^{1}D)) in CM3/CMIP5 simulations, using 20-yr averages (1860–1879 to 1986–2005 for historical, 2006–2025 to 2081–2100 for future projections). Values below 500 hPa are used for temperature, rate constant, OH, water vapor, LNO$_x$ and J(O^{1}D). Boxes are shaded only when the direction of the change in the variable matches the indicated τ_{CH_4} or OH change. Factors that increase the methane lifetime are denoted by grey shaded boxes with italic text, while black shaded boxes with italic text indicate factors that decrease the methane lifetime. Grey shaded boxes indicate factors that increase OH, while black shaded boxes indicate factors that decrease OH.

Experiment	Δτ_{CH4} (%)	ΔTEMP (K)	Δk (%)	ΔOH (%)	ΔCH$_4$ (%)	ΔCOEMIS (%)	ΔNOEMIS (%)	ΔLNO$_x$ (%)	ΔH$_2$O (%)	ΔJ(O^{1}D) (%)
HIST	5.0	0.3	0.8	-6.0	108.7	117.8	329.3	-2.5	2.0	0.74
AEROSOL	7.3	-1.0	-2.2	-4.5	0	0	0	-6.9	-5.8	-1.2
AEROSOL INDIRECT	6.9	-0.9	-2.0	-4.3	0	0	0	-4.7	-5.3	-1.2
ANTHRO	4.6	0.6	1.4	-6.6	108.7	117.8	329.3	-1.8	4.0	-1.9
NATURAL	1.4	-0.1	-0.3	-1.1	0	0	0	-1.4	-0.8	-0.8
WMGGO3	-4.3	2.0	4.6	-1.2	108.9	117.8	329.3	4.6	12.9	-0.8
RCP2.6	-9.1	1.1	2.5	7.3	-27.1	-31.1	-46.5	4.4	6.8	0.4
RCP4.5	-13.0	2.3	5.4	8.7	-9.1	-42.6	-45.1	8.2	14.8	-0.4
RCP4.5*	-5.2	1.4	3.1	2.1	0.2	0	0	2.4	8.4	0.1
RCP6.0	-5.8	2.8	6.5	-0.8	2.3	-17.8	-46.4	11.5	18.2	-1.2
RCP8.5	4.3	4.5	10.8	-14.8	97.2	-26.2	-30.2	15.0	31.1	-6.4

Title Page

Abstract | Introduction

Conclusions | References

Tables | Figures

|◄ | ►|

◄ | ►

Back | Close

Full Screen / Esc

Printer-friendly Version

Interactive Discussion

Table 6. Correlation coefficients (r) for global annual mean OH versus global annual total methane burden (CH_4), CO emissions (COEMIS), surface NO emissions (NOEMIS), and lightning NO_x (LNO_x); global annual average airmass-weighted water vapor (H_2O) and photolysis rates ($J(O^1D)$); and global total stratospheric ozone ($STRATO_3$), over the length of CM3/CMIP5 model simulation periods (146 yr for historical, 95 yr for RCPs). Values below 500 hPa are used for OH, water vapor, LNO_x and $J(O^1D)$. Boxes are shaded when they have the correct sign of r to match the sign of OH change in Table 5. Grey shaded boxes denote variables that have correct sign of r to increase OH. Black shaded boxes indicate variables that have correct sign of r to decrease OH.

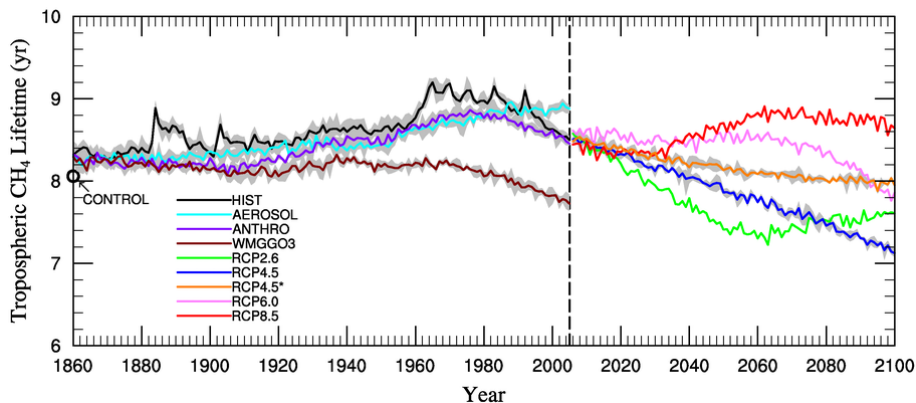| Experiment	r_CH4	r_COEMIS	r_NOEMIS	r_LNO$_x$ (below 500hPa)	r_H2O (below 500hPa)	r_J(O^{1}D) (below 500hPa)	r_STRATO$_3$
HIST	-0.84	-0.81	-0.81	0.77	-0.06	0.49	0.10
AEROSOL	0.60	N/A	N/A	0.91	0.98	0.86	-0.67
AEROSOL INDIRECT	0.57	N/A	N/A	0.82	0.96	0.84	-0.63
ANTHRO	-0.92	-0.89	-0.89	0.69	-0.44	0.91	-0.07
NATURAL	0.34	N/A	N/A	0.63	0.86	0.84	-0.84
WMGGO3	-0.67	-0.62	-0.62	-0.35	-0.57	0.82	-0.25
RCP2.6	-0.84	-0.75	-0.70	0.56	0.86	-0.19	0.87
RCP4.5	-0.85	-0.98	-0.95	0.89	0.92	-0.02	0.81
RCP4.5*	0.89	N/A	N/A	0.47	0.95	0.07	0.73
RCP6.0	-0.97	0.08	0.28	-0.08	-0.30	0.75	-0.57
RCP8.5	-0.99	0.99	0.98	-0.84	-0.96	0.96	-0.97

Fig. 1. Evolution of global annual mean tropospheric methane lifetime (yr) in GFDL CM3/CMIP5 simulations: HIST (black), AEROSOL (cyan), ANTHRO (purple), WMGGO3 (brown), RCP2.6 (light green), RCP4.5 (dark blue), RCP4.5* (orange), RCP6.0 (pink), RCP8.5 (red). Grey shaded regions indicate the range of ensemble members.

Title Page

Abstract | Introduction

Conclusions | References

Tables | Figures

|◄ | ►|

◄ | ►

Back | Close

Full Screen / Esc

Printer-friendly Version

Interactive Discussion

**Climate versus
emission drivers of
methane lifetime**

J. G. John et al.

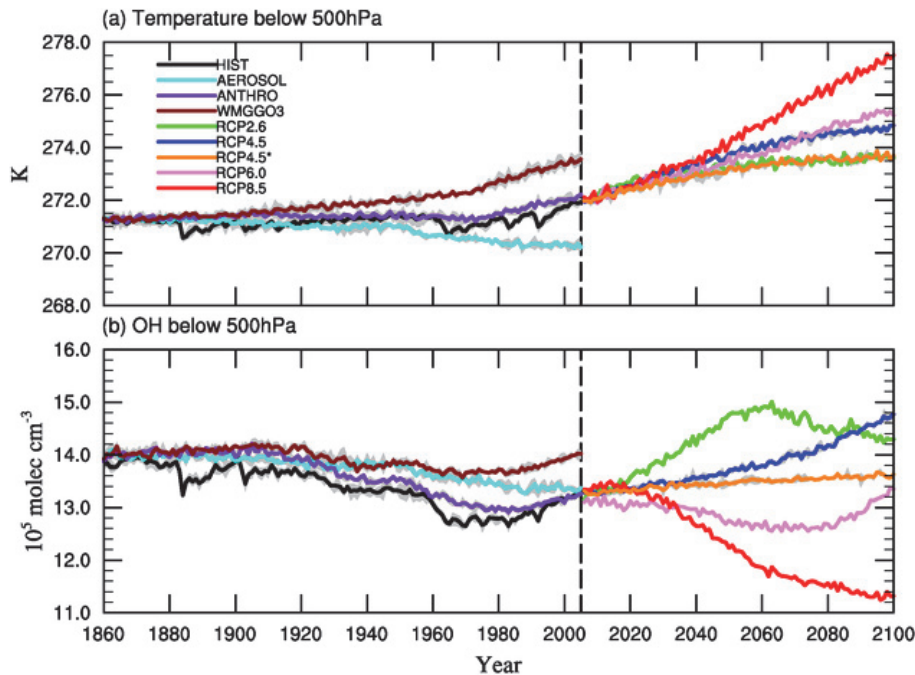**Fig. 2.** Percent change in methane lifetime ($\Delta\tau_{CH_4}$) versus sum of percent change in rate constant (Δk) and OH (ΔOH) in CM3/CMIP5 simulations, using 20-yr averages from 1860–1879 to 1986–2005 for historical simulations, and from 2006–2025 to 2081–2100 for future projections. Colored diamonds: HIST (black), AEROSOL (cyan), AEROSOL INDIRECT (blue), ANTHRO (purple), NATURAL (dark green), WMGGO3 (brown), RCP2.6 (light green), RCP4.5 (dark blue), RCP4.5* (orange), RCP6.0 (pink), RCP8.5 (red).

Fig. 3. Trajectories of global annual average airmass-weighted **(a)** temperature below 500 hPa (K) and **(b)** OH below 500 hPa (10^5 molec cm^{-3}) in CM3/CMIP5 simulations. Grey shaded regions indicate the range of ensemble members. Colored lines: HIST (black), AEROSOL (cyan), ANTHRO (purple), WMGGO3 (brown), RCP2.6 (light green), RCP4.5 (dark blue), RCP4.5* (orange), RCP6.0 (pink), RCP8.5 (red).
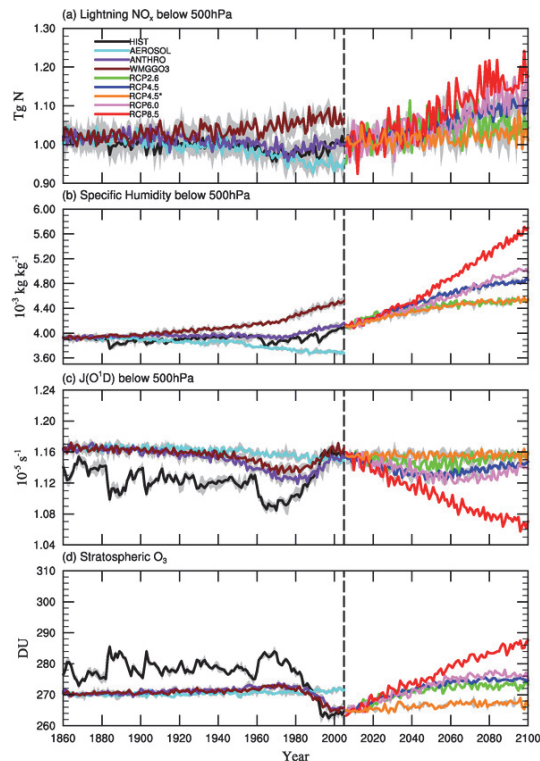
Fig. 4. Evolution of **(a)** global annual total lightning NO_x (Tg N), global annual average airmass-weighted **(b)** specific humidity (H_2O, 10^{-3} kg kg^{-1}) and **(c)** photolysis rate ($J(O^1D)$, 10^{-5} s^{-1}), and **(d)** global annual total stratospheric ozone (DU) in CM3/CMIP5 simulations. LNO_x, H_2O and $J(O^1D)$ are all below 500 hPa. Grey shaded regions indicate the range of ensemble members. Colored lines: HIST (black), AEROSOL (cyan), ANTHRO (purple), WMGGO3 (brown), RCP2.6 (light green), RCP4.5 (dark blue), RCP4.5* (orange), RCP6.0 (pink), RCP8.5 (red).

Title Page

Abstract | Introduction

Conclusions | References

Tables | Figures

◀ | ▶|

◀ | ▶

Back | Close

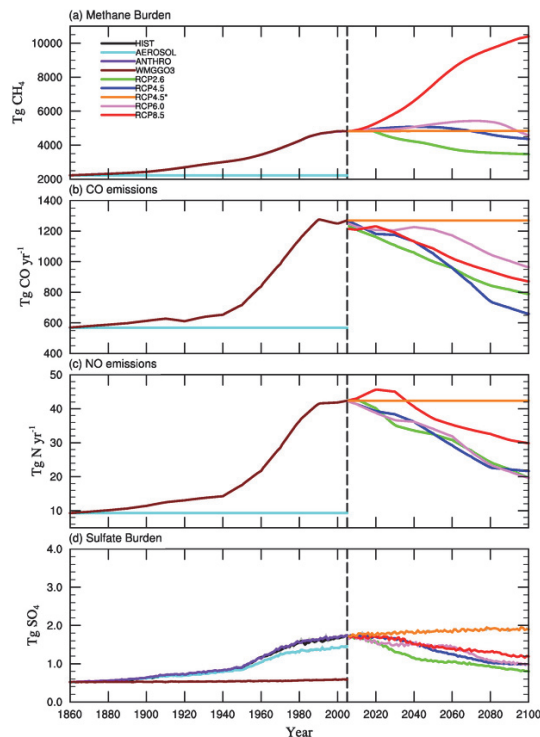Full Screen / Esc

Printer-friendly Version

Interactive Discussion

Fig. 5. Evolution of global annual total **(a)** methane burden ($Tg\,CH_4$) **(b)** CO emissions ($Tg\,CO\,yr^{-1}$) **(c)** NO emissions ($Tg\,N\,yr^{-1}$) and **(d)** sulfate burden ($Tg\,SO_4$) in CM3/CMIP5 simulations. Grey shaded regions indicate the range of ensemble members. Colored lines: HIST (black), AEROSOL (cyan), ANTHRO (purple), WMGGO3 (brown), RCP2.6 (light green), RCP4.5 (dark blue), RCP4.5* (orange), RCP6.0 (pink), RCP8.5 (red).